Electronics Supplementary Information

Pseudo-Boehmite AlOOH/NGr Composite-Based Air Electrode for Mechanically Rechargeable Zn-Air Battery Applications

Geeta Pandurang Kharabe,[a, b] Narugopal Manna,[a, b] Ayasha Nadeema, [c] Santosh K. Singh,[d] Shweta Mehta, [a, b] Aathira Nair, [a, b] Kavita Joshi,*[a, b] Sreekumar Kurungot,*[a, b]

(a) Geeta Pandurang Kharabe, Narugopal Manna, Shweta Mehta, Aathira Nair, Kavita Joshi, Dr. Sreekumar Kurungot

Physical & Materials Chemistry Division, CSIR-National Chemical Laboratory. Pune, Maharashtra; Email: k.sreekumar@ncl.res.in

(b) Geeta Pandurang Kharabe, Narugopal Manna, Shweta Mehta, Aathira Nair, Dr. Kavita Joshi, Dr. Sreekumar Kurungot

Academy of Scientific and Innovative Research, Postal Staff College Area, Kamla Nehru Nagar, Ghaziabad, Uttar Pradesh-201002.

(c) Dr. Ayasha Nadeema, Department of Energy Science and Engineering, IIT Bombay.

(d) Dr. Santosh K. Singh, Department of Chemistry, School of Natural Science, Shiv Nadar University, Uttar Pradesh-201314, India.

Table of Contents

1. Experimental Section

1.1. Physical Characterization: Bulk morphological investigations and compositional information were investigated through field-emission scanning electron microscopy (FE-SEM) using FEI Nova Nano SEM 450 FE-SEM instrument. FEI, TECNAI G2 F-20 transmission electron microscopy (TEM) instrument at an accelerating voltage of 200 kV was used for the nanostructural imaging. FESEM samples were prepared by dispersing the obtained material in isopropyl alcohol (IPA) (5 mg of sample in 1 ml IPA) *via* bath-sonication; then the dispersed sample was coated on a silicon wafer. The sample was dried for 1 h under an IR lamp. High-resolution imaging and HAADF−STEM mapping were performed using a JEOL JEM F-200 HRTEM instrument. The samples for TEM and HRTEM analysis were prepared by dropwise coating of the well-dispersed sample in isopropyl alcohol (1.0 mg of the sample in 5 mL IPA) over a carbon-coated 200 mesh copper grid. The drying of the TEM grid was performed by exposing under an IR lamp for 1 h. To unravel the crystallinity and phase purity characteristics of the as-prepared samples, X-ray diffraction (XRD) analysis was performed on a Rigaku Smart Lab X-ray diffractometer (Cu Kα radiation (λ=1.5406 Å); scan rate of 2° min^{-1}; 2θ range of 10 to 80°). Raman spectral investigations were performed using 632 nm green laser (NRS 1500W) on a HR 800 RAMAN spectrometer. Active material loading in the NGr-supported samples was investigated by using thermogravimetric analysis (TGA) (SDT Q600 DSC-TDA thermo-gravimetric instrument; temperature range of 10-900 °C; ramp of 10 min^{-1}°C ; oxygen atmosphere). The information on the presence of the elements, their respective chemical environments, and binding energy was gathered with the help of X-ray photoelectron spectroscopy (XPS) experiments. A VG Micro-Tech ESCA 300° instrument was employed for the XPS measurements.

1.2. Computational Details:

All the calculations are carried out within the Kohn-Sham formalism of Density Functional Theory. Projector Augmented Wave potential is used, with Perdew-Burke-Ernzerhof (PBE) approximation for the exchange-correlation and generalized gradient approximation, as implemented in plane-wave, pseudo-potential based code, Vienna Ab initio Simulation Package (VASP).[1] We modeled graphene nano-sheet with supercell size of 5x5 resulting into 50 carbon atoms. To mimic the experiments, pyridinic N is introduced which is the most dominant defect on the graphene and henceforth will be referred as NGR. The AlOOH unit is placed at all unique sites viz. top, bridge, and center of the hexagonal ring. Van der Waals corrections are applied to account for dynamic correlations between fluctuating charge distribution by employing

Grimme method (DFT-D2). It is observed that 20 Å of vacuum is sufficient to avoid interaction between adjacent images of graphene along the z-direction. Geometry optimization is carried out with a force cutoff of 0.01 eV/Å and the total energies are converged below 10^{-4} eV for each SCF cycle. A Monkhorst-Pack grid of 5x5x1 for pristine and N doped graphene is used. To compare the interaction of AlOOH at these sites, interaction energy is calculated using the formula: $E_{ads} = E_{system} - (E_{surface} + E_{AlOOH})$ where E_{system} is energy of the system when AlOOH is placed on the graphene/NGR, $E_{surface}$ is energy of the bare surface and E_{AlOOH} is energy of the AlOOH molecule. The electronic structure of these systems is analyzed by computing projected Density of States (pDOS) with denser k-mesh using LOBSTER along with Mulliken charges for all the atoms on the surface.[2]

1.3 Electrochemical Analysis:

Electrochemical experiments required for the present study were carried out using a Bio-Logic potentiostat (model VMP-3). A set of electrochemical techniques such as rotating disk electrode (RDE), rotating ring disk electrode (RRDE), cyclic voltammetry (CV), linear sweep voltammetry (LSV) etc. were employed for collecting various information pertaining to the electrochemical characteristics of the materials. The tests were performed in a standard three-electrode system consisting of a catalyst-coated glassy carbon electrode (GCE, a diameter of 0.19625 mm), graphite rod and a saturated Hg/HgO as the working electrode, counter electrode and reference electrode, respectively.

1.3.1. Rotating Disk Electrode Study: The electrochemical performance was evaluated by performing a set of electrochemical techniques, including cyclic voltammetry (CV) and linear sweep voltammetry (LSV) using a Pine Instrument in the RDE mode. First, a three-electrode electrochemical cell was used to study the half-cell reactions with an SP-300 model Bio Logic potentiostat. The as-synthesized catalysts were coated over a working electrode by making a catalyst ink followed by its coating on the electrode. The Hg/HgO was used as a reference electrode and a graphite rod (Alfa Aesar, 99.99%) was employed as a counter electrode. ORR activity measurement was performed in oxygen-saturated aqueous 0.1 M KOH solution. Pt/C was employed as the reference catalyst for comparing the ORR performance. The catalyst slurry was prepared by mixing the catalyst (5 mg) in 1 mL isopropyl alcohol-water (1:2) solution and 40 µL of Nafion solution (5 wt%, Sigma-Aldrich) using water-bath sonication for approximately 1 h. After the formation of catalyst slurry, the 10 µL of the slurry (final loading of catalyst = 50 µg cm^{-2}) was drop-casted on the surface of the glassy carbon electrode (0.196 cm^{-2}), which was polished with 0.3 µm alumina slurry in DI-water followed by cleaning with DI-water and acetone. The electrode was subsequently dried under an IR-lamp for 1 h. All the experimental electrode potentials were converted into the reversible hydrogen electrode (RHE) scale through an RHE calibration experiment which is given in section 1.2.3.

1.3.2. Rotating Ring Disk Electrode Study: In the case of the RRDE analysis of the prepared catalysts, the catalyst coated disc electrode of the RRDE was scanned at a scan rate of 10 mV s^{-1} while keeping the ring electrode at a constant potential of 0.40 V *vs.* Hg/HgO. At first, collection efficiency (N) at the ring was determined with a $K_3Fe(CN)_6$ solution, which is found to be 0.37.[3] The calculation of H_2O_2% and the number of electron transfer (n) during the ORR was carried out by following the equations below:

$$\% \text{ hydrogen peroxide} = 200\times(I_R*N)/(I_D+I_R/N)$$

$$n = 4\times I_D/(I_D + I_R/N)$$

where,

I_D = Faradaic current at the disk

I_R = Faradaic current at the ring

N = H_2O_2 collection efficiency of the ring electrode

All the electrochemical experiments were carried out at room temperature.

1.3.3. The Hg/HgO reference electrode calibration and conversion to RHE:

The calibration of the Hg/HgO electrode has been performed according to our previous report.[3] The experiment was performed by utilizing a 3-electrode setup consists of a platinum RDE electrode, graphite rod, and Hg/HgO as the working electrode (WE), counter electrode (CE), and reference electrode (RE), respectively, in an H_2-saturated 0.1M KOH electrolyte. The potential at which the current crossed the zero point during the linear sweep voltammogram (LSV) measurement at a scan rate of 0.50 mV/s was measured and this point has been taken as the thermodynamic potential for the calibration purpose. This potential was found to be 0.87 V, and, hence, the conversion of the voltage recorded as for Hg/HgO to the RHE scale has been done by using the following equation:

$$E\ (\text{RHE}) = E\ (\text{Hg/HgO}) + 0.87\ \text{V} \quad \ldots\ldots 1$$

1.4. Zinc-Air Battery (ZAB) Fabrication and Testing:

Fabrication of the ZAB was performed by using a Zn foil and AlOOH/NGr as the anode and the cathode electrodes, respectively, and the testing was done in an in-house-built electrochemical cell. Subsequent to sonication of AlOOH/NGr for 35 min and probe sonication for 10 min in isopropyl alcohol, Fumion and DI water solution, the catalyst slurry was coated on the gas diffusion layer (GDL). The catalyst loading was maintained as 1.0 mg/cm^2 (electrode area = 1.0 cm^2), and the catalyst-coated GDL was dried at 60 °C for 12 h. The as-obtained cathodes and the Zn anode were cut into 1*3 cm^2 areas; with the help of a Teflon tape, an exposed electrode area of 1*1 was maintained for the measurements. Finally, the ZAB was assembled by pairing the anode and cathode using 6.0 M KOH, where only 1*1 cm^2 of the active electrodes was allowed to expose. The ZAB setup was subsequently tested at room temperature using a multichannel SP-300 model Bio-Logic potentiostat/galvanostat. The battery was analyzed by steady-state polarization measured with the same setup under the continuous purging of oxygen at a potential scan rate of 5 mV s^{-1}.[4]

Fig. S1: (b) SEM-EDX mapping of (a) NGr (b) AlOOH/NGr.

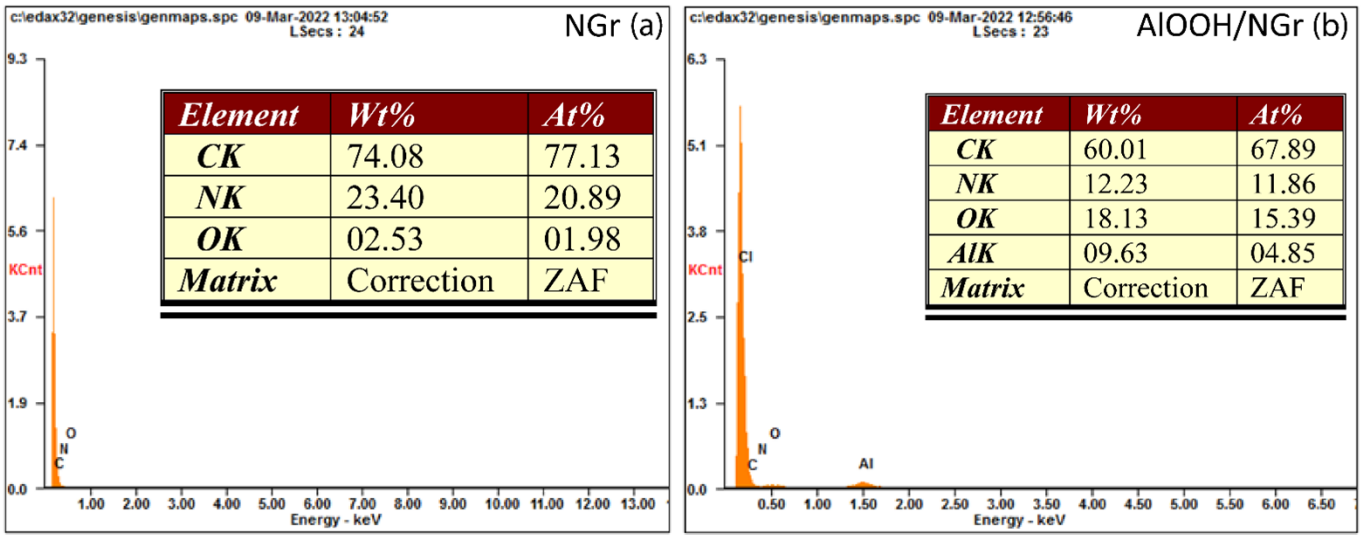

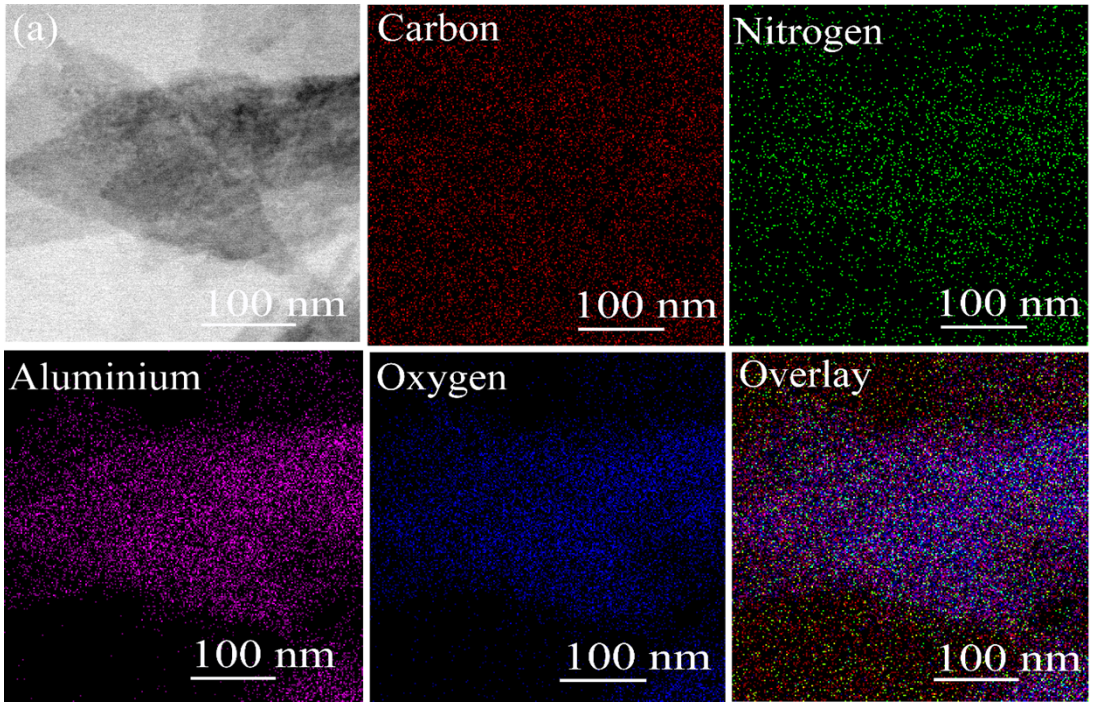

Fig. S2. (a) HRTEM image selected for the elemental mapping. Elemental mapping images for C (red), N (green), Al (magenta) and O (blue) elemental overlapping image for C, N, O and Al present in AlOOH/NGr.

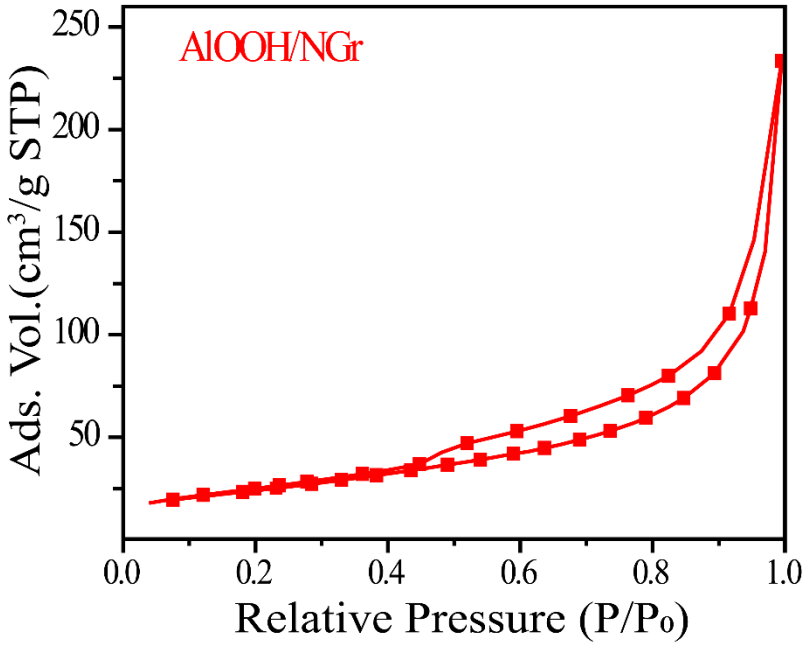

Fig. S3: Nitrogen adsorption/desorption isotherms of AlOOH/NGr.

1.5. Oxygen Reduction Mechanism:

In alkaline medium, two pathways are generally proposed for the ORR; one route follows through a direct four-electron pathway, and the second is a two-electron pathway. Also, as a third possibility a sequential four (2+2) electron pathway has also been proposed. These pathways are comprised of multiple elementary steps:[5]

1. The direct 4e− pathway in the oxygen reduction process involves the conversion of O_2 to OH^-:
   $O_2 + 2H_2O + 4e^- \rightarrow 4OH^-$ [1]

2. On the other hand, the $2e^-$ pathway converts O_2 to HO_2^-:

   $O_2 + H_2O + 2e^- \rightarrow HO_2^- + OH^-$ $E_0 = -0.076$ V *vs* SHE [2]

3. The HO_2^- be converted to OH^-, following a further $2e^-$ reduction to OH^- (a sequential four-electron pathway):

   $HO_2^- + H_2O + 2e- \rightarrow 3OH^-$ $E_0 = 0.878$ V vs SHE [3a]

4. As another possibility, the HO_2^- can be desorbed from the catalyst surface and undergo disproportionation ($2e^-$ ORR pathway):

   $2HO_2^- \rightarrow 2OH^- + O_2$ [3b]

Generally, the four-electron transfer, either following a direct or sequential pathway, is preferable in the case of the electrochemical devices.[6] This necessitates the designing with an aim to catalyze the $4e^-$ reduction of O_2 to OH^-. In this context, here we are pointing out some of the key characteristics of our chosen material which support the correlations between the physicochemical characteristics of the designed catalyst as well as its potential to catalyze the ORR:

1. The positively charged surface of AlOOH favors the oxygen adsorption and subsequent ORR.

2. Hydroxides are more stable than the transition metal oxides in alkaline solution.

3. According to the DFT study, the AlOOH is found to be more stable over NGr than on graphene.

Also, according to some literature, oxyhydroxide-based catalysts can facilitate the four-electron selective pathway in an alkaline electrolyte. The ORR performance depends upon the kinetics of the redox reaction as well as the redox potential of the catalyst. During the O_2 reduction *via* the 4-electron transfer pathway, the oxyhydroxide supplies electrons to the oxygen atom absorbed on the MOOH surface.[7] It subsequently induces oxidation of hydroxide to form oxyhydroxide. The oxyhydroxide then converts back to the hydroxide to complete the 4-electron ORR process.

The 4e⁻ pathway ORR reaction on AlOOH/NGr in alkaline medium is described as below,[8-10]

$* + O_2(g) + H_2O(l) + e^- \rightarrow OOH^* + OH^-$ (1)

$OOH^* + e^- \rightarrow O^* + OH^-$ (2)

$O^* + H_2O(l) + e^- \rightarrow OH^* + OH^-$ (3)

$OH^* + e^- \rightarrow OH^- + *$ (4)

where, * represents an adsorption site and X* represents the adsorption intermediate on the surface.

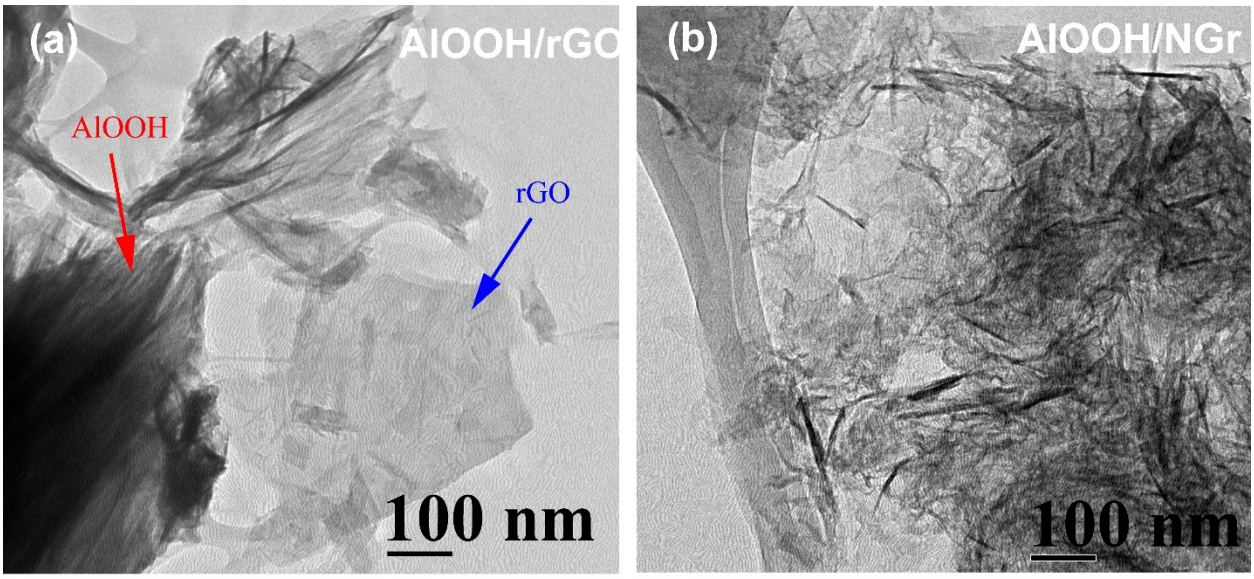

Fig. S5: TEM analysis: (a) AlOOH/rGO and (b) AlOOH/NGr.

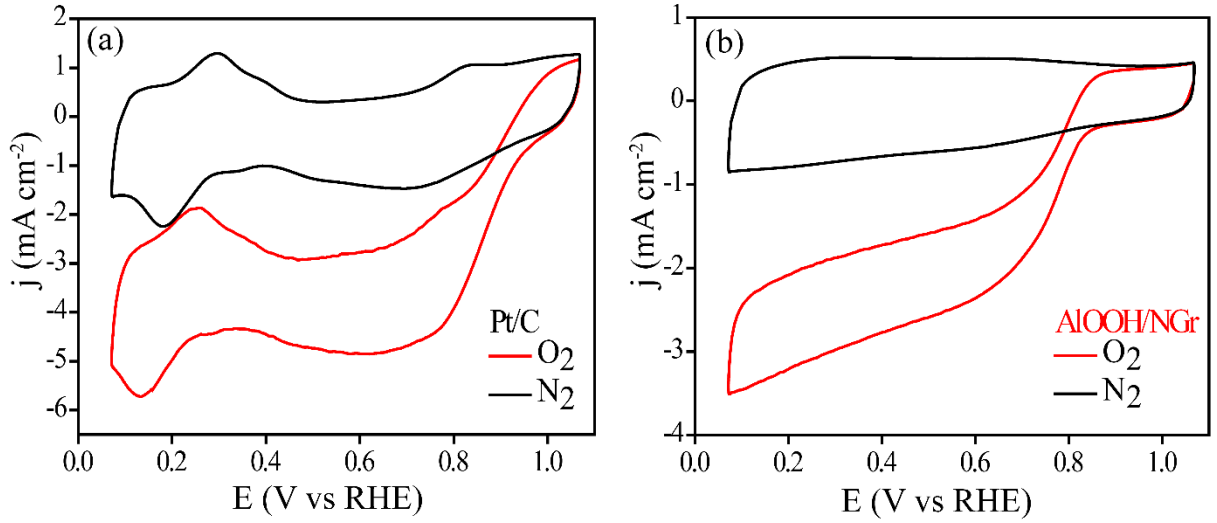

Fig. S6: Cyclic voltammograms of (a) Pt/C and (b) AlOOH/NGr, recorded at a scan rate of 50 mV s−1 in N2-saturated (black line) and O2-saturated (red line) 0.1 M KOH solution.

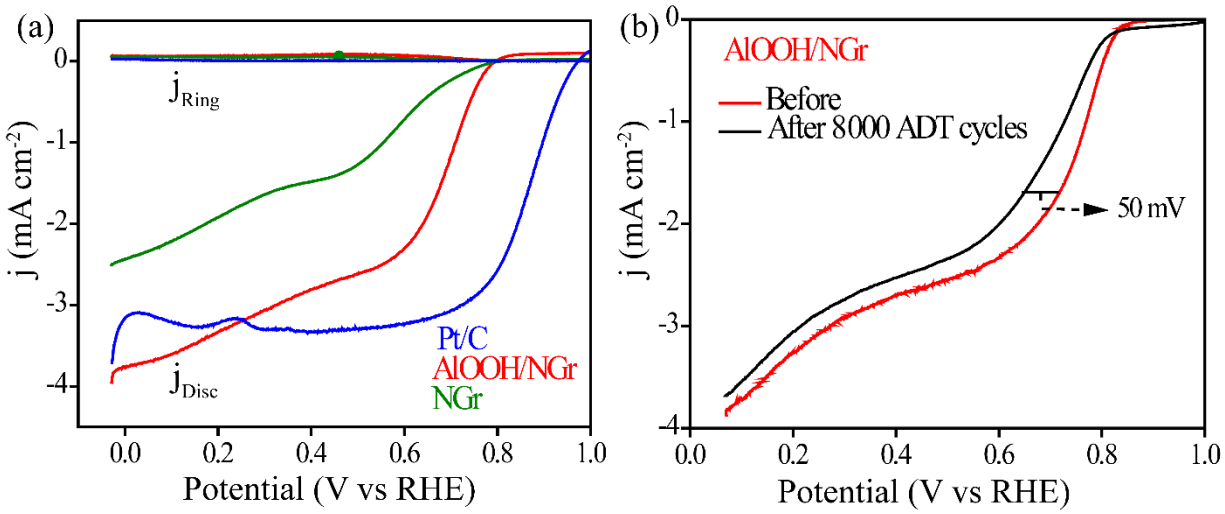

Fig. S7: (a) RRDE plot for ring and disk current analyis of NGr, AlOOH/NGr and Pt/C catalayst and (b) LSVs recorded before and after the 8000 CV cycles for AlOOH/NGr .

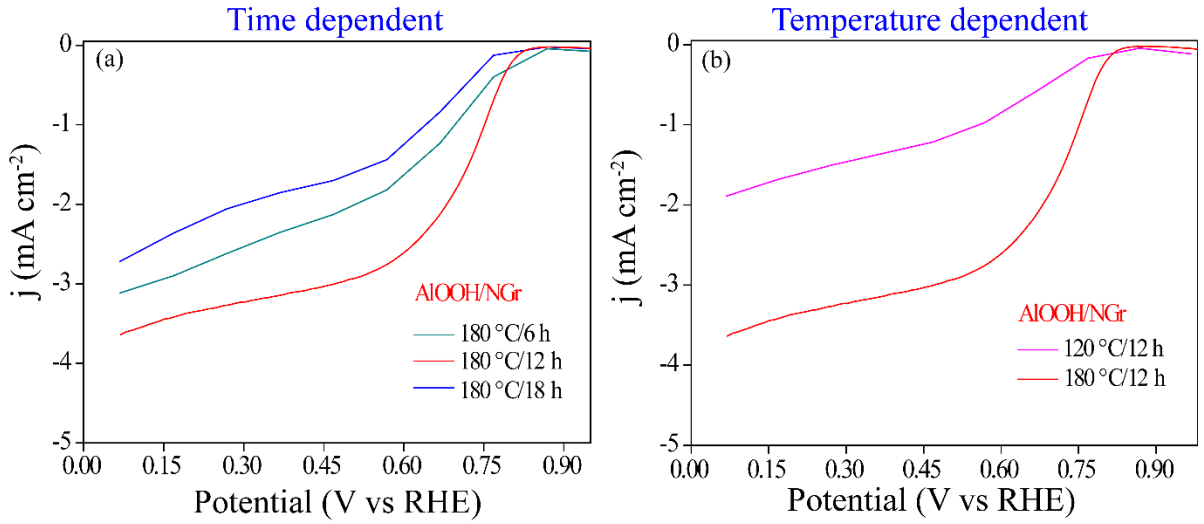

Fig. S8: Electrochemical analysis of the catalysts in 0.1 M KOH: (a) the LSVs recorded over the catalysts prepared at different reaction durations while maintaining constant reaction temperature of 180 °C; (b) the comparative LSVs of AlOOH.NGr prepared at 120 and 180 °C at the reaction duration of 12 h.

Table S1: Onset (E) and half-wave ($E_{1/2}$) potentials recorded for the time and temperature dependent synthesized catalysts.

AlOOH/NGr	**Onset Potential (E)**	**Half-wave Potential ($E_{1/2}$)**
120 °C/12 h	0.79 V	0.55 V
180 °C/6 h	0.84 V	0.62 V
180 °C/12 h	0.83 V	0.72 V
180 °C/18 h	0.78 V	0.78 V

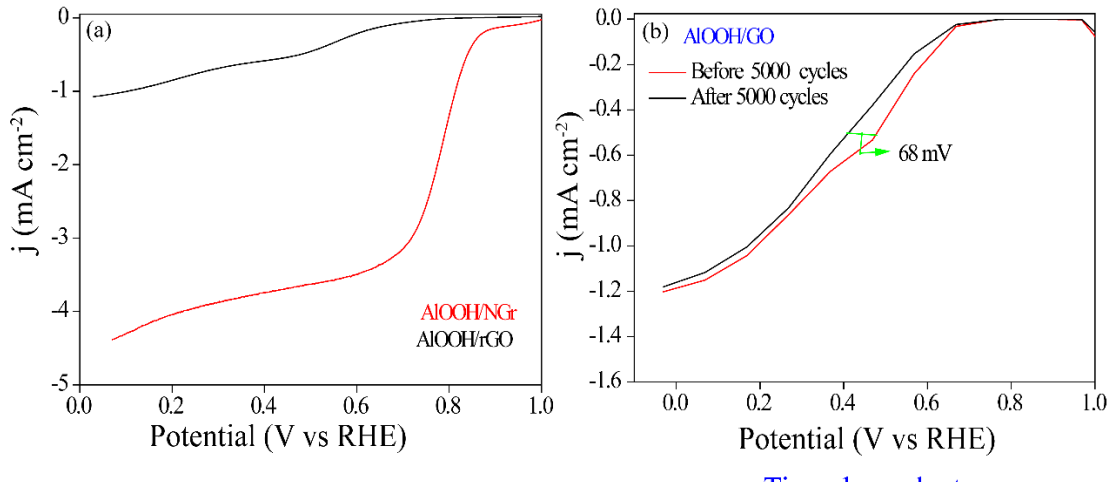

Fig. S9: (a) The comparative LSV profiles of AlOOH/NGr and AlOOH/rGO recorded in 0.1 M KOH; (b) the LSV profiles recorded before and after the durability analysis of AlOOH/GO.

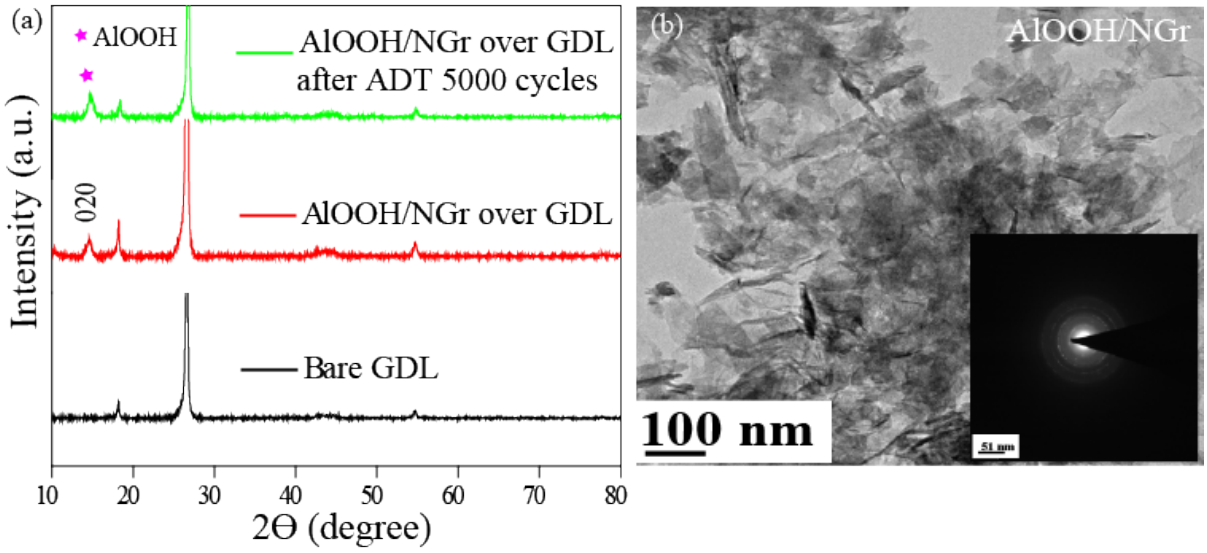

Fig. S10: (a) Comparative XRD pattern, and (b) TEM image of the cycled catalyst, (inset: SAED pattern).

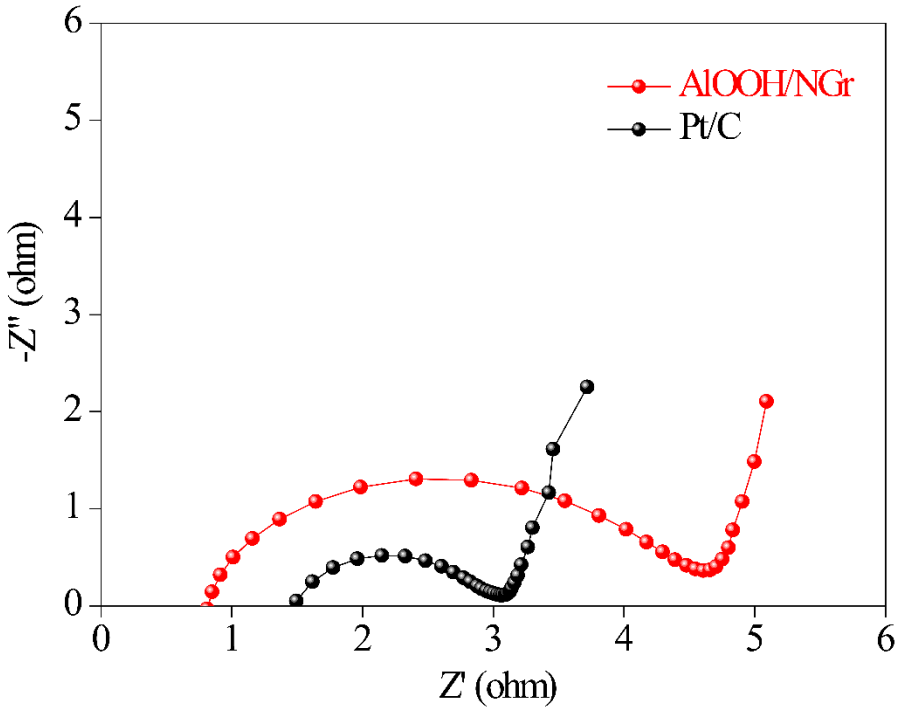

Fig. S11: The comparative Nyquist plots recorded for AlOOH/NGr and Pt/C based ZABs under the OCV condition.

The step-by-step process of mechanical rechargeability of our in-house battery system.

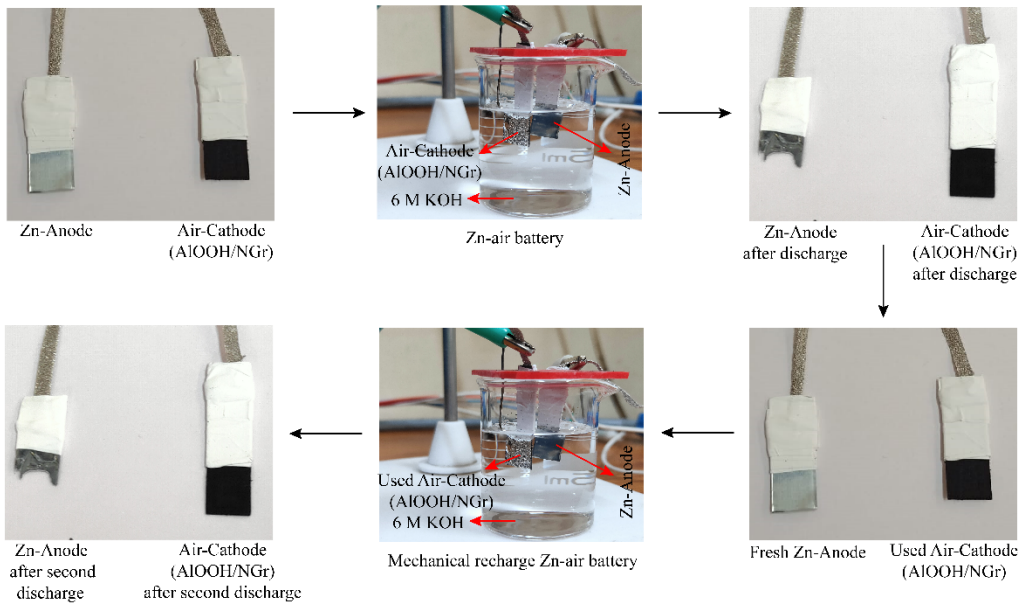

Fig. S12: Pictorial representation of step-by-step process involving in the mechanical recharging of the in-house battery system.

Table S2: Onset (E) and half-wave ($E_{1/2}$) potentials recorded for the various synthesized catalysts.

Sample	Onset Potential (V *vs.* RHE)	Half-Wave Potential (V *vs.* RHE)
NGr	0.70 V	0.54 V
AlOOH/NGr	0.83 V	0.72 V
Pt/C	0.98 V	0.84 V

Table S3: Comparison of the ORR activities of the reported systems in the literature *vs* the in-house systems.

Sr. No.	Electrocatalyst	Onset Potential (V *vs.* RHE)	Half-Wave Potential (V *vs.* RHE)	Tafel Slope (mV dec^{-1})	References
1.	CuPt-NC	0.95 V	0.846 V	~69.94	11
2.	Co/N-C-800	0.83 V	0.74V	NA	*12*
3.	Co3O4/NEGF	0.94 V	0.84 V	74	*13*
4.	**AlOOH/NGr**	**0.83 V**	**0.72 V**	**~69**	**Present invention**

Table S4: Comparison of the key performance indicators of the various ZABs reported in the literature with the present work.

Sr.	Electrocatalyst	Power density	Specific capacities	Current densities	References

No.			(mAh/gm-$_{Zn}$)	(mA/cm^2)	
1.	CoO/N-CNT	265 mW cm^{-2}	NA	~200 mA/ cm^2	*3*
2.	CuPt/NC	NA	560 mAh /g_{Zn}	20 mA/ cm^2	*11*
3.	Co_3O_4/NEGF	210 mW/cm^2	490 mAh /g_{Zn}	10 mA/ cm^2	*13*
4.	CF-N-rGO-150	540 mW/cm^2	630 mAh /g_{Zn}	20 mA/ cm^2	*14*
5.	**AlOOH/NGr**	**204 mW/cm^2**	**703 mAh /g_{-Zn}**	**10 mA/ cm^2**	**Present invention**

2. References

1. Kresse, G.; Furthmüller, J., Efficiency of ab-initio total energy calculations for metals and semiconductors using a plane-wave basis set. *Computational Materials Science* **1996,** *6* (1), 15-50.
2. Maintz, S.; Deringer, V. L.; Tchougréeff, A. L.; Dronskowski, R., LOBSTER: A tool to extract chemical bonding from plane-wave based DFT. **2016,** *37* (11), 1030-1035.
3. Singh, S. K.; Kashyap, V.; Manna, N.; Bhange, S. N.; Soni, R.; Boukherroub, R.; Szunerits, S.; Kurungot, S., Efficient and Durable Oxygen Reduction Electrocatalyst Based on CoMn Alloy Oxide Nanoparticles Supported Over N-Doped Porous Graphene. *ACS Catalysis* **2017,** *7* (10), 6700-6710.
4. Li, Y.; Gong, M.; Liang, Y.; Feng, J.; Kim, J.-E.; Wang, H.; Hong, G.; Zhang, B.; Dai, H., Advanced zinc-air batteries based on high-performance hybrid electrocatalysts. *Nature Communications* **2013,** *4* (1), 1805.
5. Ge, X.; Sumboja, A.; Wuu, D.; An, T.; Li, B.; Goh, F. W. T.; Hor, T. S. A.; Zong, Y.; Liu, Z., Oxygen Reduction in Alkaline Media: From Mechanisms to Recent Advances of Catalysts. *ACS Catalysis* **2015,** *5* (8), 4643-4667.
6. Scholz, F.; Kahlert, H., The calculation of the solubility of metal hydroxides, oxide-hydroxides, and oxides, and their visualisation in logarithmic diagrams. *ChemTexts* **2015,** *1* (1), 7.
7. Jia, N.; Liu, J.; Liu, Y.; Wang, L.; Chen, P.; An, Z.; Chen, X.; Chen, Y., In situ conversion of iron sulfide (FeS) to iron oxyhydroxide (γ-FeOOH) on N, S co-doped porous carbon nanosheets: An efficient

electrocatalyst for the oxygen reduction reaction and zinc–air batteries. *Journal of Colloid and Interface Science* **2020,** *558*, 323-333.
8. Lu, J.; Yang, L.; Guo, W.; Xiao, S.; Wang, L.; OuYang, Y.; Gao, P., The mechanism of Co oxyhydroxide nano-islands deposited on a Pt surface to promote the oxygen reduction reaction at the cathode of fuel cells. *RSC Advances* **2020,** *10* (73), 44719-44727.
9. Liu, X.; Hu, W., Iron oxide/oxyhydroxide decorated graphene oxides for oxygen reduction reaction catalysis: a comparison study. *RSC Advances* **2016,** *6* (35), 29848-29854.
10. Vandichel, M.; Laasonen, K.; Kondov, I., Oxygen Evolution and Reduction on Fe-doped NiOOH: Influence of Solvent, Dopant Position and Reaction Mechanism. *Topics in Catalysis* **2020,** *63* (9), 833-845.
11. Dhavale, V. M.; Kurungot, S., Cu–Pt Nanocage with 3-D Electrocatalytic Surface as an Efficient Oxygen Reduction Electrocatalyst for a Primary Zn–Air Battery. *ACS Catalysis* **2015,** *5* (3), 1445-1452.
12. Su, Y.; Zhu, Y.; Jiang, H.; Shen, J.; Yang, X.; Zou, W.; Chen, J.; Li, C., Cobalt nanoparticles embedded in N-doped carbon as an efficient bifunctional electrocatalyst for oxygen reduction and evolution reactions. *Nanoscale* **2014,** *6* (24), 15080-15089.
13. Manna, N.; Singh, S. K.; Kharabe, G. P.; Torris, A.; Kurungot, S., Zinc–Air Batteries Catalyzed Using Co3O4 Nanorod-Supported N-Doped Entangled Graphene for Oxygen Reduction Reaction. *ACS Applied Energy Materials* **2021,** *4* (5), 4570-4580.
14. Kashyap, V.; Singh, S. K.; Kurungot, S., Cobalt Ferrite Bearing Nitrogen-Doped Reduced Graphene Oxide Layers Spatially Separated with Microporous Carbon as Efficient Oxygen Reduction Electrocatalyst. *ACS Applied Materials & Interfaces* **2016,** *8* (32), 20730-20740.